An in-vacuum, pixelated detection system for mass spectrometric analysis and imaging of macromolecules

Julia H. Jungmann[1], Donald F. Smith[1], Andras Kiss[1], Luke MacAleese[1,+], Ronald Buijs[1], Ron M.A. Heeren[1]

[1] *FOM Institute AMOLF, Science Park 104, 1098 XG Amsterdam, The Netherlands*

+ current affiliation: Institut Lumière Matière, UMR5306 Université Lyon 1-CNRS, Université de Lyon 69622, Villeurbanne Cedex, France

The analytical capabilities of a Timepix detection system for mass spectrometry (imaging) are extended by the application of additional acceleration fields. Electrically biasing the detection system at a high potential delivers effective ion acceleration energies of 15/11 keV for positive/negative ion mode matrix-assisted laser desorption ionization. This is comparable to the acceleration/extraction fields in commercially available time-of-flight mass spectrometers. This high voltage detector system enables measurements in both ion polarities and more sensitive analysis of higher molecular mass ions. The technical implementation of this system and first results in positive and negative ion mode are presented. The high voltage enhanced analytical capabilities of the Timepix detection system are demonstrated in the mass range up to 100 kDa.

Address reprint requests to Ron M.A. Heeren, FOM-Institute AMOLF, Science Park 104, 1098 XG Amsterdam, The Netherlands, Tel: +31-20-7547 161, Fax: +31-20-7547 290, E-Mail: heeren@amolf.nl

Key words: mass spectrometry imaging, microscope mode, MCP, pixelated detector, Timepix, MALDI, in-vacuum mounting, high voltage, gigabit read-out, high *m/z*, multiplexed TDC, high spatial resolution, intact protein, imaging mass spectrometry

1. Introduction

The analysis of large biomedically relevant macromolecules by mass spectrometry and mass spectrometry imaging [1, 2] is highly challenging and interesting for various applications. The reliable and sensitive detection of high-mass ions, in particular large proteins, protein complexes, viruses and bacterial clusters, would provide the life sciences with a powerful analytical tool, which could also find future applications in routing (bio)medical analysis and diagnosis. While technology for efficient ion generation and accurate mass analysis has actively and rapidly developed over the past century, technology for ion detection –particularly of high mass macromolecular complexes- has been lagging behind [3].

A few examples of high mass detection by electrospray ionization (ESI) in combination with Fourier transform ion cyclotron resonance mass spectrometry (FT-ICR MS) or time-of-fight (TOF) MS have been reported. Chen and coworkers have detected coliphage T4 DNA ions of 100 MDa on an FT-ICR MS [4]. Sanglier and co-workers have detected 2.2 MDa native hemocyanins from deep-sea and shore crabs with ESI in combination with a TOF and quadrupole time-of-flight (Q-TOF) mass analyzer [5]. Rose and co-workers have analyzed intact protein assemblies in native-like states with molecular weights approaching 1 MDa with an Orbitrap mass analyzer and ESI [6]. Similarly, DiFilippo has measured intact viral particles of the tobacco mosaic virus at 40.5 MDa with ESI-TOF [7]. Fuerstenau and co-workers reported ESI-TOF MS on macromolecules in the MDa range [8]. Doussinau and co-workers analyze megadalton to gigadalton species by ESI charge-detection MS [9]. Electrospray ionization is very efficient for the detection of high mass ions, since it readily produces multiply charged species, which can be detected more easily. However, matrix-assisted laser desorption/ionization (MALDI), as a “soft" ionization technique, is generally considered a more appropriate choice of ionization source for large intact macromolecules. MALDI is also suitable for mass spectrometry imaging where the lateral organization of the analytes from the sample surface is retained.

Detection systems for MALDI-MS, specifically with regards to mass spectrometry imaging (MSI), are often based on microchannel plates (MCP). A limitation of this secondary-electron multiplier, however, is the so-called “high-mass roll-off” of the detector. In a MCP, the ion detection depends on the generation of secondary electrons. The generation of a secondary electron avalanche is proportional to the momentum of the incoming particle. As all particles in a TOF-MS are given the same kinetic energy, high mass ions will impinge on the detector with a relatively lower momentum than lower mass ions. Hence, they may not deposit sufficient energy to create an electron shower. As a result, high mass ions are not easily detected.

Alternative detection systems for high-mass measurements with MALDI TOF-MS have been developed. Park and co-workers presented an inductive detector specifically for MALDI TOF-MS, whose detection efficiency is not ion velocity dependent and does not saturate at high count rates [10]. Imrie and co-workers reported the detection of ions above 300 kDa with a Faraday cup detector on a MALDI TOF-MS [11]. Spengler and co-workers used a metallic conversion dynode for ion detection/conversion and observed that the detection efficiency of large molecules from MALDI can benefit from optimization for secondary-ion yield rather than secondary-electron detection [12]. This approach is similar to the commercially available Covalex detector [13, 14], which routinely detects

immunoglobulin IgM (*m/z*=973.26 kDa). Cryogenic detectors are another approach to the detection of high mass ions [15-17].

In this paper, the technical implementation of a Timepix-based detection system for higher mass molecular ions of both polarities is presented. This system is both suitable for MS and MSI experiments and is implemented on an ion microscope mass spectrometer [18]. In previous Medipix 2- and Timepix-based setups for MS(I) [19-21], the pixelated detector was held at ground potential. Therefore, the imaging system was limited in its ability to analyze high-mass ions by the acceleration voltage. The upgraded detector assembly presented here is operated at a floating voltage of +12 kV/-8 kV. This provides high voltage (HV) post-acceleration capabilities for both ion polarities. Previously, only positive mode ion imaging of basic and/or salt adduct species was possible with the MCP/Timepix detection system on this ion microscope. The extension to negative mode ion imaging enables the study of acidic species, which enables the analysis of different moieties, i.e. different lipids, acidic peptides and proteins. Therefore, the capability to study a tissue sample in both positive and negative mode provides complementary information on biological systems. In addition, the higher post-acceleration voltages provide the capability to detect higher mass intact proteins in both polarities.

Several technical challenges are related to the in-vacuum mounting of the Timepix detector. In earlier work, detectors of the Medipix/Timepix detector family were mounted in-vacuum including substantial parts of the readout electronics in the vacuum chamber [19, 22, 23]. Here, the implementation of a new, high vacuum-compatible chip carrier is presented for the first time. This multifunctional chip carrier acts both as a vacuum seal and high-density, electrical feedthrough. As a result, the chips are mounted in-vacuum while the readout electronics are located in air outside of the vacuum chamber. The in-vacuum mounting of the Timepix chips requires active cooling of the in-vacuum components of the system as to prevent overheating. Experimental results in positive and negative ion mode and protein detection in the mass range up to 100 kDa are presented.

2. Materials and Methods

2.1. The Medipix/Timepix Detectors. The Medipix/Timepix detector family is developed by the Medipix collaboration hosted by CERN (Medipix collaboration, www.cern.ch/medipix). The Medipix2 [24, 25]/Timepix [26] chips in combination with a detection medium, typically a semiconductor like silicon or cadmium telluride, are hybrid, active pixel detectors. In the semiconductor sensor layer, incident particles are converted into electron-hole pairs, which can induce a charge in the charge-sensitive amplifier of the complementary metal oxide semiconductor (CMOS) read-out chip. The energy of the incident particle, typically X-rays or electrons, determines the number of created charge carriers. Ions are typically not accelerated sufficiently to penetrate into the sensor layer. Ions can be detected by placement of an MCP in front of the read-out chip [27]. The chip then detects electron showers produced by ion impacts on the MCP.

The dimension of an individual Medipix/Timepix chip is 1.4 × 1.6 cm^2. The application-specific integrated circuit (ASIC) consists of 256×256 pixels of 55 × 55 μm^2 each. In the Timepix chip, each pixel can be individually selected to operate in one of three modes: (1) the counting mode, in which

each pixel counts the number of impinging particles; (2) the time-of-flight (TOF) mode, in which the arrival time of one impinging particle is measured with respect to an external trigger/shutter signal; (3) the time-over-threshold (TOT) mode, in which the time is measured during which a fired pixel stays over the detection threshold. Different pixels can be operated in different modes. The chip is controlled via a dedicated acquisition and control software and graphical user interface, “Pixelman” [28, 29]. The Medipix2/Timepix chips and their areas of application are reviewed elsewhere [30].

2.2. Mass spectrometers. The Timepix detection system is mounted on a TOF ion microscope. The ion microscope is a TRIple Focusing Time-of-flight (TRIFT II) mass spectrometer (Physical Electronics, Inc., Chanhassen, USA). The TRIFT mass spectrometer delivers an ion optical magnification of a factor of 40× to 100×. Hence, a 55×55 μm^2 detector pixel corresponds to, respectively, areas of 1.38×1.38 μm^2 and 550×550 nm^2 on the sample surface. The details of ion microscope mass spectrometers is covered in detail elsewhere [18, 31]. On this ion microscope, a 2×2 chip Timepix detector is installed 2 mm behind a ϕ = 4 cm chevron microchannel plate. The pores of the MCP have a diameter of 12 µm on a 15 µm center-to-center spacing. The system is normally operated at a constant MCP gain of 10^7 and with a potential difference of 900 V between the MCP backside and the Timepix detector. These voltage settings are tuned for optimal electron shower sizes for both spatial resolution and spectral quality. The MCP-Timepix detector assembly is mounted on the ion microscope using a specifically developed, high-vacuum compatible chip carrier and vacuum seal, which is described below. Reference measurements to test the Timepix-generated spectra are taken with the time-to-digital converter of the TRIFT II and with an Ultraflex III MALDI TOF(/TOF)-MS (Bruker Daltonik GmbH, Bremen, Germany).

2.3. High Voltage Post-Acceleration Capabilities: Detector Floating on +12/-8 kV. The implementation of the Timepix detector on our ion microscope aims at efficient, position- and time-/mass-resolved analysis of complex biological samples for molecular histology. In earlier Medipix-/Timepix-based imaging systems, the detector was held at ground potential [19-21]. Therefore, the detection system was limited to post-acceleration voltages of about 5 kV, i.e. applied by the sample potential of +3 kV and the MCP front bias of -2 kV. In addition, the experiments were limited to the positive ion mode.

To enable the detection of higher mass ions in both ion polarities, the entire Timepix detector assembly, including the chips, readout electronics, power supplies and cooling system, is floating at a voltage of about +12 kV (in negative ion mode) and -8 kV (in positive ion mode). This provides high voltage post-acceleration capabilities for both ion polarities and allows for the analysis of very high mass macromolecular ions. Fig. 1 displays a potential diagram for the operation of the floating Timepix detector assembly in positive and negative ion mode. Since the Timepix detector assembly is floating at HV, it has to be electrically insulated and shielded from the mass spectrometer and surroundings. Fig. A.1 and A.2 (Appendix A), respectively, illustrate the mechanical and electrical design of the setup, which contains two cylindrical shells: (1) the “inner" setup shell, which is floated at HV and (2) the “outer", which is held at ground potential. The floating detector assembly is attached to the mass spectrometer via an electrically isolated ceramic tube. The MCP/Timepix detector assembly, the ReLAXD readout board [32, 33], the cooling system (Peltier elements, temperature controller, cooling fans) and mechanical parts in the inner setup shell are all floated at HV. The floating HV is applied to the inner detector shell from the standard TRIFT II power supplies of

the ion microscope via a home-made converter situated in the outer/ground potential setup shell. The MCP back- and front side are powered by the original TRIFT MCP power supplies. A decoupling circuit for the MCP backside signal is in place for signal diagnostics on an oscilloscope or to acquire mass spectra with the Timepix system or an ADC/TDC. The ReLAXD board, the Peltier elements, the temperature controller and the fans are powered by two home-made, switching mode power supplies which are located within the inner detector shell and are also floating at HV. Since the Ethernet signal from the ReLAXD board is at HV, the signal line has to be electrically insulated to enable the signal transfer into a PC at ground potential. Therefore, the Ethernet signal is translated by an optical fiber protocol via a media converter (Ntron Industrial Ethernet media converter, 1002MC-SX, N-Tron Corporation, Mobile, USA). The non-conducting optical fiber is sent out of the HV setup and the signal is reconverted to the Ethernet protocol via another optical-to-Ethernet media converter. The signal is then coupled to the Ethernet card of the measurement/control personal computer.

2.4. High-Vacuum Compatible Chip Carrier and Vacuum Seal. The Medipix/Timepix detector assemblies and readout electronics are not originally designed for in-vacuum use. The chips are normally mounted on a printed circuit board (PCB) to which another readout PCB is connected. The PCBs are made up of multiple, outgassing FR-4 (flame retardant 4; fiberglass reinforced epoxy laminates) layers and other non-vacuum compatible electronics components. In earlier proof-of-principle experiments, the Medipix/Timepix detectors and readout electronics were mounted either directly in the spectrometer chamber or in a differentially pumped vacuum chamber. This resulted in typical spectrometer pressures of $P=10^{-7}$ mbar [19, 22]. Despite the increased spectrometer pressure, the benefits of a new generation of imaging detectors in mass spectrometry imaging and gas-phase atomic and molecular physics research could be established in these experiments [19, 22] .

Here, a new, ultra-high-vacuum compatible chip carrier (Fig. 2) and vacuum seal are presented (Fig. 3) that increase the performance and applicability of the Medipix/Timepix detectors in ultra-high vacuum applications, like MS(I). The carrier acts as a seal between the vacuum of the mass spectrometer and the in-air components of the system. The chips are mounted in-vacuum, while the readout electronics are located in-air outside the vacuum chamber. The chip carrier also consists of a standard, multilayer FR-4 PCB. This carrier supports the chips and connects the chips with the readout interface PCB. The FR-4 PCB is coated with Liquid Crystalline Polymer Circuit material (LCP, R/ex 3600 Single Clad Laminate, Rogers Corporation, Advanced Circuit Materials, Chandler, USA) on both sides which prevents the PCB from out-gassing. This material has successfully been applied as a coating for high-vacuum parts in mass spectrometry [34]. The use of standard PCB material bears the advantages of easy, economical, reliable and well-established electrical design and fabrication. In addition, PCBs can be manufactured in various shapes (rectangular versus circular) and sizes (from few mm up to tens of cm in diameter). In this application, the PCB is circular in shape, has a diameter of about 50 mm and a thickness of about 1.6 mm. The edges of the PCB are (partly) beveled under an angle of 45^{o} for optimal vacuum sealing in the stainless steel mount. Since the PCB is only coated with LCP on the top and bottom surfaces, the board can outgas via its edges. Therefore, the edges of the board are sealed with a layer of copper (Cu) and indium (In). To ensure the temperature control of the chips, thermal vias are distributed all over the PCB. In addition, a Max6642 (Maxim Integrated Products, Inc., Sunnyvale, USA) temperature sensor is incorporated in the PCB which allows to monitor the temperature of the chips at all times.

The presented chip carrier is mounted in a stainless steel support (Fig. 3). Since the LCP-coated chip carrier represents a vacuum seal of this system, the connection between the chip carrier and the stainless steel support needs to be vacuum-tight. The support is machined such that the beveled edge of the chip carrier can be glued (vacuum-compatible, two-component silver epoxy, Hysol TRA-DUCT 2902, Henkel, Duesseldorf, Germany) into the stainless steel support (Fig. 3a), which is beveled at the same angle. This vacuum seal was tested on a leak tester (130 l/s hybrid turbo-molecular pump, ASM 180T, Alcatel, Annecy, France). A leak rate of less than $P=10^{-9}$ mbar l/s was measured. The helium testing gas could not be detected at an inlet speed of 4.4 l/s, (smallest detectable signal at full pumping speed is $5.1\cdot10^{-12}$ mbar l/s).

The chip carrier is mechanically supported by a copper disc (Fig. 3b), which prevents mechanical stress due to the pressure difference between the vacuum on the chip-side of the carrier and the ambient pressure on the electronics-side of the board. The chip carrier and the copper support disc are connected by an electrically and thermally conducting, two-component silver epoxy glue (EPO-TEK EE129-4, Epoxy Technology, Inc. , Billerica, USA). This copper disc also functions as a heat sink and connects the chip carrier to the active Peltier element-based cooling system. The stainless steel support of the carrier is connected to the mass spectrometer by a ϕ=1.5 mm indium thread (Degussa, Hanau, Germany). The combination of the two seals returns the same leak rate, i.e. less than $P=10^{-9}$ mbar l/s, and the helium leak testing gas still could not be detected.

The detector system was assembled through the following procedure: (1) glue the chip carrier to the copper cooling disk and into its stainless steel support, (2) probe the Timepix chips (quality control), (3) glue the Timepix chips to the chip carrier, (4) wire-bond the chips, (5) mount assembly via indium seal, (6) leak test assembly, (7) install the chip carrier vacuum assembly on the TRIFT ion microscope. The spectrometer was baked for 48 hours with the standard bakeout procedure of the TRIFT II spectrometer system, i.e. with external heating straps in combination with internal infrared bakeout lamps. The heating strap closest to the detection system was located on the adapter flange between the spectrometer and the detector setup (Fig. A.1). The detector setup beyond the connecting ceramics tube (Fig. A.1) was not baked out to prevent overheating of the chip-based detection system. After bakeout a spectrometer pressure of $P=2\cdot10^{-9}$ mbar could be established. This represents an improvement of almost two orders of magnitude compared to previous efforts ($P=10^{-7}$ mbar) which had involved differential pumping or in-vacuum mounting of the readout electronics. Further, a temperature read-back and control system has been designed (details in Appendix B).

2.5. Samples. A protein sample with analytes in the mass range from about 5-8.5 kDa was prepared from Bruker Protein Calibration Standard I (Bruker Daltonik GmbH, Bremen, Germany, Table 1) and spotted on an indium-tin-oxide (ITO) coated glass slide (Delta Technologies, Loveland, USA). The protein solution was mixed 1:1 (by volume) with sinapinic acid matrix solution (20 mg/ml in 50% water (0.1% trifluoracetic acid), 50% acetonitrile) and spots of 1 µl were spotted on the ITO slide. A second protein sample with analytes in the mass range from 5-66.5kDa was prepared from a 1:1 Protein Calibration Standard I and Protein Calibration Standard II (Bruker Daltonik GmbH, Bremen, Germany, Table 1) on an ITO coated glass slide. The protein solution was mixed 1:1 (by volume) with sinapinic acid matrix solution as described above and spots of 1 µl were spotted on the ITO slide and air dried at room temperature. A sample of the protein ubiquitin was prepared. A solution of 1 mg/ml ubiquitin (Sigma-Aldrich, St. Louis, USA; 50% ACN, 0.1% TFA) and 20 mg/ml sinapinic acid

(Fluka Analytical, now Sigma-Aldrich, St. Louis, USA; 50% ACN, 0.1% TFA) was homogeneously sprayed onto an ITO slide with a Bruker ImagePrep device (Bruker Daltonik GmbH, Bremen, Germany). Ubiquitin has a $[M+H]^+$ average mass of 8565.76 Da.

3. Results and Discussion

3.1. Negative Ion Mode. Negative ion mode mass spectra of the protein calibration standard in the mass range from 0-15 kDa as a function of ion acceleration energy from 4-13 keV are shown in Figs. 4a and 4b. The total ion acceleration energy is calculated by the sum of initial kinetic energy given to the ions in the source of the mass spectrometer (3 keV) plus the post-acceleration voltage at the detector (2-10 keV for singly charged ions, see Fig. 1). Each spectrum is generated from a single mosaic mode acquisition of 5,000 frames, i.e. 5,000 laser shots. The mosaic acquisition rasters a sample area of 0.9×0.9 mm^2 with 16×16 positions. This method ensures that every measurement covers the same size of sample area. Also, the mosaic mode acquisition averages out hot spots on the sample surface. In the mass range up to 15 kDa, the calibration standard includes three protein peaks; insulin ($[M-H]^-$=5,732.51), ubiquitin I ($[M-H]^-$=8,563.76) and cytochrome C ($[M-H]^-$=12,358.97). These peaks are clearly observed in the spectra at all ion post-acceleration energies. Fig. 4a demonstrates that the intensity of the signal (peak and baseline) increases as a function of the ion post-acceleration voltage (the initial kinetic energy of the ions in the source region was held constant at 3 keV). Note that the amount of ions generated in the source region is independent of the post-acceleration voltage. However, the increase in the signal intensity can be explained by the fact that an increased ion kinetic energy at the detector results in an increased ion momentum for a given ion mass. The higher ion momentum upon impact on the MCP increases the probability of creating the first electron needed to start an electron avalanche in the MCP. If the first electron is created, the MCP amplification (10^7) is sufficient to ensure detection on the Timepix pixels, since only approximately 650 electrons are required to fire a pixel. It is expected that the increase in signal with a higher extraction field levels off or is not observed at higher count rates and/or higher post-acceleration voltages, since the number of available pixels on the Timepix is finite. Each pixel is a single-stop TDC, thus if the count rate is high at normal acceleration voltage (here, 3 keV), then the extra counts due to the increased post-acceleration voltage will not be registered if all of the pixels in the field of view have been triggered already.

Fig. 4b displays the time-of-flight spectrum[1] of the protein calibration standard in the mass range of about 10-18 kDa acquired in negative ion mode at ion acceleration energies of 7-13 keV. In this mass range, the calibration standard includes two protein peaks; cytochrome C and myoglobin ($[M-H]^-$ =16,950.30). Both peaks could be detected in the Timepix-generated spectra at ion acceleration energies exceeding 7 keV. At lower ion acceleration energies no significant peaks (signal-to-noise ratio > 3) could be detected in this mass range. This proves that the combination of a MCP/Timepix detection system with additional post-acceleration fields enables sensitive negative-ion mode mass spectrometric analysis where the use of Timepix chips, in addition to the MCP, allows for highly parallel, multiplexed event detection as compared to MCP-only detection systems.

[1] A time-of-flight spectrum instead of a mass spectrum is displayed to illustrate the peak shifts observed as a function of the ion acceleration energy. This effect is commented on in 3.2.

3.2. Positive Ion Mode. Fig. 4c shows positive ion mode mass spectra of the protein calibration standard in the mass range from 0-14.5 kDa as a function of the total ion acceleration energy (5.5-13 keV for singly charged ions). The spectra shows the peaks of the proteins insulin ($[M+H]^+$=5,734.51), ubiquitin ($[M+H]^+$=8,565.76) and cytochrome C ($[M+H]^+$=12,360.97), as well as lower mass peaks in the mass range m/z<4,000. Interestingly, the intensities of the protein peaks (insulin, ubiquitin, cytochrome C) decrease with increasing post-acceleration voltages on the detector, i.e. with increasing ion acceleration energies. In the lower mass region (m/z<4,000) the inverse is observed, the intensities of the peaks increase with increasing post-acceleration voltages on the detector. This effect is related to the ion load on the detection system in combination with the single-stop TDCs in the Timepix pixels. The count rates in these positive mode measurements are high, i.e. (nearly) all pixels within the field of view detect an event even at the lowest ion acceleration energy (5.5 keV). With increasing ion acceleration energies, the ion momentum increases and the probability to produce a hit (and induce an electron shower) on the MCP increases per ion. Since the Timepix pixels are single-stop TDCs (i.e. once fired the pixels are blind for events arriving later during the same measurement interval), this gives a detection advantage to lower mass (earlier arrival time) ions. In high count rate measurements, higher post-acceleration voltages result in spectra where the lower mass signal is enhanced (as observed in the mass range m/z<4,000 of Fig. 4c) and where the higher mass signal is decreased (as observed for the protein peaks in Fig. 4c).

Fig. 4d shows the time-of-flight spectra of the protein calibration standard in the mass range of about 10-18 kDa acquired in positive ion mode at ion acceleration energies of 5.5-13 keV. The cytochrome C and the myoglobin ($[M+H]^+$=12,360.97 and $[M+H]^+$=16,952.30) peaks can be detected in the Timepix-generated spectra. A clear increase of the signal with the increasing ion acceleration energy is observed, since the count rates in these measurements are sufficiently low to enable additional counts on previously “unused" pixels. The higher mass protein spectrum is displayed as a time-of-flight instead of a mass spectrum. In this representation, it becomes apparent that the peaks of the proteins are being shifted to a shorter time-of-flight as a function of the post-acceleration voltage. This phenomenon can be explained by the increased post-acceleration applied to the ions. As indicated in Fig. 1, the ion acceleration is composed of two acceleration stages, i.e. the initial acceleration at the sample stage (~3kV) and the final acceleration behind the mass spectrometer towards the detector (2-10 kV) in the post-acceleration region. The magnitude of the post-acceleration field determines the final time-of-flight of the ions.

3.3. Wide mass range spectral capabilities. The performance of the HV detection system over a large mass range is evaluated with a protein sample in the mass range ≤ 70 kDa (Table 1). The protein calibration standard was measured in positive ion mode for ion acceleration energies of 5.5 keV and 10.5 keV (Fig. 5). Fig. 5 displays the raw Timepix-generated spectra. As reported in [20], the bit depth of the Timepix detector limits the time-of-flight measurements to about 118 µs at a 10 ns clock cycle resolution. Hence, large mass range spectra have to be recorded in successive portions (for TOF ranges > 118 µs), which are acquired by delaying the Timepix measurement interval with respect to the ion-generating laser shot. To cover the mass range of the protein standard, the spectra displayed in Fig. 5 consist of four consecutive, raw spectra which correspond to 5,000 laser shots each. The Timepix detection system gives a detection advantage to lower mass ions since the Timepix pixels are single-stop TDCs. Hence, consecutive ions with a longer time-of-flight are not “seen” by a pixel which has previously been occupied in a measurement cycle [21]. This results in high ion counts at low mass

and gradually lower ion counts towards higher masses in high count rate regimes where many pixels are occupied multiple times (as discussed in "positive ion mode" above). This effect results in "bumps" in the "stitched" wide mass range spectra (in Fig. 5, for instance, around 15 kDa where two spectral portions are stitched together), i.e. , there are relatively less ions detected towards the end of spectrum portion *n* while there are relatively more ions detected at the beginning of spectrum portion *n+1*. This effect can be reduced by moderating the ion count rate or by smoothing algorithms.

A comparison between the spectra at ion acceleration energies of 5.5 keV and 10.5 keV shows the analytical advantage that the higher post-acceleration voltage delivers. The BSA^{2+} peak at 33,300 Da is more pronounced at the higher post-acceleration voltage. The protein A^{+} peak at 44,613 Da is detected in the spectrum acquired at the 10.5 keV ion acceleration energy but not at lower post-acceleration voltages. A comparison with the standard time-to-digital converter (TDC) of the TRIFT system is included in Appendix C (Fig. C.1). The protein standard was measured with the TDC system for ion acceleration energies of 5.5 keV, 8 keV and 10.5 keV. The increased ion acceleration energy does not result in additional analytical capabilities with the TDC. A comparison of the Timepix-generated and the TDC-generated spectra of the protein standard shows that with the TDC only a mass range of up to 33 kDa (BSA^{2+}) is accessible, while the Timepix still detects Protein A^{+} at 44.6 kDa. Further, the signal-to-noise ratio of the raw TDC signal is poor compared to the sharp Timepix-generated spectra. The Timepix-generated spectra are compared to spectra acquired with an Ultraflex III MALDI TOF-MS (Fig. C.2). The Ultraflex spectra were generated in linear ion mode with an ion acceleration energy of 25 keV. Note that the ions are accelerated by an initial ion extraction in the Ultraflex, while the acceleration in the Timepix system is composed of the initial extraction and a post-acceleration (Fig. 1). Fig. C.2 displays the raw Ultraflex spectrum (no baseline subtraction) as acquired with the standard Ultraflex system analog-to-digital converter. The Timepix- and Ultraflex-generated spectra are generally comparable, even though the Ultraflex' ion acceleration energy is about twice that of the Timepix.

The accessible mass range is further investigated with a sample of the protein ubiquitin. Fig. 6 displays two spectra acquired at ion acceleration energies of 5.5 keV and 10.5 keV. The wide mass range is composed of four measurements of 5,000 laser shots each which have been stitched together, as outlined above. The higher post-acceleration voltage spectrum shows spectral features in the mass range up to 100 kDa, which represents the maximum mass range accessible with the TRIFT spectrometer (hardware/software limitations due to secondary ion mass spectrometry nature of the instrument), while the lower post-acceleration voltage spectrum displays distinct spectral features up to about 80 kDa [20]. The 10.5 keV spectrum shows ubiquitin up until its 11-mer at 94.2 kDa, which illustrates that the full mass range of the TRIFT spectrometer is accessible with the Timepix detection system.

4. Conclusions

We described a high voltage Timepix-based detection system for MS(I). This system extends the already established advantages of the Timepix, i.e. position- and time-sensitive measurements, measurement of different masses simultaneously, high dynamic range, high throughput and high

spatial resolution [19-21], towards the detection of high *m/z* species. The experiments presented here establish ion detection capabilities in both positive and negative ion mode, which provides the capability to collect complementary analytical information. The initial experiments indicate that the ion signal is enhanced with an increased post-acceleration voltage in moderate count rate regimes. Future studies should investigate the signal increase as a function of the post-acceleration voltage in different count rate regimes, which will provide systematic experimental guidelines for the optimum application of post-acceleration voltages for the presented detection system. It was established that the Timepix detection system benefits from increased ion post-acceleration voltages for both spectral quality and accessing a mass range up to 100 kDa. This system enables positive and negative mode MALDI TOF-MSI in the microscope mode, with the added capability of high mass detection (i.e. intact proteins).

Acknowledgements

Part of this research is supported by the Dutch Technology Foundation STW, which is the applied science division of NWO, and the Technology Programme of the Ministry of Economic Affairs, Project OTP 11956. This work is part of the research program of the "Stichting voor Fundamenteel Onderzoek der Materie (FOM)", which is financially supported by the "Nederlandse organisatie voor Wetenschappelijk Onderzoek (NWO)". The authors thank the Medipix collaboration hosted by CERN, in particular, our colleagues Henk Boterenbrood, Marten Bosma, Joop Rövekamp, Bas van der Heijden, Jan Koopstra, Jan Visser and Jan Visschers (FOM-Institute Nikhef, Amsterdam). We also thank Xavi Llopart and Michael Campbell (CERN, Geneva), Marc Duursma, Frans Giskes, Henk Neerings, Dirk-Jan Spaanderman and Sjoerd Wouda (AMOLF) for their contribution to this work. We thank Erika Amstalden van Hove for help with the Ultraflex MALDI-TOF measurements.

References

[1] L.A. McDonnell, R.M.A. Heeren, Mass spectrometry imaging, Mass Spectrom. Rev., 26 (2007) 606-643.
[2] K. Chughtai, R.M.A. Heeren, Mass Spectrometric Imaging for Biomedical Tissue Analysis, Chemical Reviews, 110 (2010) 3237-3277.
[3] J.H. Jungmann, R.M.A. Heeren, Emerging technologies in mass spectrometry imaging, Journal of Proteomics, (2012).
[4] R.D. Chen, X.H. Cheng, D.W. Mitchell, S.A. Hofstadler, Q.Y. Wu, A.L. Rockwood, M.G. Sherman, R.D. Smith, Trapping, detection, and mass determination of coliphage T4 DNA ions of 10(8) Da by electrospray-ionization Fourier-transform ion-cyclotron resonance mass-spectrometry Analytical Chemistry, 67 (1995) 1159-1163.
[5] S. Sanglier, E. Leize, A. Van Dorsselaer, F. Zal, Comparative ESI-MS study of similar to 2.2 MDa native hemocyanins from deep-sea and shore crabs: From protein oligomeric state to biotope, J. Am. Soc. Mass Spectrom., 14 (2003) 419-429.
[6] R.J. Rose, E. Damoc, E. Denisov, A. Makarov, A.J.R. Heck, High-sensitivity Orbitrap mass analysis of intact macromolecular assemblies, Nature Methods, 9 (2012) 1084–1086.
[7] F. DiFilippo, V. Natarajan, M. Bradley, F. Palmer, D.E. Pritchard, Accurate atomic mass measurements from Penning trap mass comparisons of individual ions Physica Scripta, T59 (1995).
[8] S.D. Fuerstenau, W.H. Benner, Molecular weight determination of megadalton DNA electrospray ions using charge detection time-of-flight mass spectrometry, Rapid Communications in Mass Spectrometry, 9 (1995) 1528-1538.
[9] T. Doussineau, C.Y. Bao, R. Antoine, P. Dugourd, W.J. Zhang, F. D'Agosto, B. Charleux, Direct Molar Mass Determination of Self-Assembled Amphiphilic Block Copolymer Nanoobjects Using Electrospray-Charge Detection Mass Spectrometry, ACS Macro Lett., 1 (2012) 414-417.
[10] M.A. Park, J.H. Callahan, An Inductive Detector for Time-of-Flight Mass-Spectrometry, Rapid Communications in Mass Spectrometry, 8 (1994) 317-322.
[11] D.W. Chandler, P.L. Houston, Two-dimensional imaging of state-selected photodissociation products detected by multiphoton ionization, Journal of Chemical Physics, 87 (1987) 1445-1447.
[12] B. Spengler, D. Kirsch, R. Kaufmann, M. Karas, F. Hillenkamp, U. Giessmann, The Detection of Large Molecules in Matrix-Assisted Uv-Laser Desorption, Rapid Communications in Mass Spectrometry, 4 (1990) 301-305.
[13] R.J. Wenzel, S. Kern, R. Zenobi, Proceedings of the 54th ASMS Conference on Mass Spectrometry and Allied Topics, Seattle, USA, (2006).
[14] A. van Remoortere, R.J.M. van Zeijl, N. van den Oever, J. Franck, R. Longuespee, M. Wisztorski, M. Salzet, A.M. Deelder, I. Fournier, L.A. McDonnell, MALDI Imaging and Profiling MS of Higher Mass Proteins from Tissue, J. Am. Soc. Mass Spectrom., 21 (2010) 1922-1929.
[15] H. Kraus, Cryogenic detectors and their application to mass spectrometry, Int. J. Mass Spectrom., 215 (2002) 45-58.
[16] M. Frank, S.E. Labov, G. Westmacott, W.H. Benner, Energy-sensitive cryogenic detectors for high-mass biomolecule mass spectrometry, Mass Spectrometry Reviews, 18 (1999) 155-186.
[17] M. Frank, Mass spectrometry with cryogenic detectors, Nucl. Instrum. Methods Phys. Res. Sect. A-Accel. Spectrom. Dect. Assoc. Equip., 444 (2000) 375-384.
[18] S.L.M. Luxembourg, T.H.; McDonnell, L.A.; Heeren, R.M.A. , High-Spatial Resolution Mass Spectrometric Imaging of Peptide and Protein Distributions on a Surface, Anal. Chem., 76 (2004) 5339-5344.
[19] J.H. Jungmann, L. MacAleese, R. Buijs, F. Giskes, A. de Snaijer, J. Visser, J. Visschers, M.J.J. Vrakking, R.M.A. Heeren, Fast, High Resolution Mass Spectrometry Imaging Using a Medipix Pixelated Detector, J. Am. Soc. Mass Spectrom., 21 (2010) 2023-2030.
[20] J.H. Jungmann, L. MacAleese, J. Visser, M.J.J. Vrakking, R.M.A. Heeren, High Dynamic Range Bio-Molecular Ion Microscopy with the Timepix Detector, Analytical Chemistry, 83 (2011) 7888-7894.

[21] Julia H. Jungmann, Donald F. Smith, Luke MacAleese, Ivo Klinkert, Jan Visser, R.M.A. Heeren, Biological Tissue Imaging with a Position and Time Sensitive Pixelated Detector, J. Am. Soc. Mass Spectrom., (2012).
[22] G.H. Gademann, Y.; Gijsbertsen, A.; Jungmann, J.; Visschers, J.; Vrakking, M.J.J Velocity map imaging using an in-vacuum pixel detector, Rev. Sci. Instrum., 8 (2009).
[23] C. Bamberger, U. Renz, A. Bamberger, Digital Imaging Mass Spectrometry, J. Am. Soc. Mass Spectrom., 22 (2011) 1079-1087.
[24] X.C. Llopart, M.; Dinapoli, R.; San Segundo, D.; Pernigotti, E. , Medipix2, a 64k pixel readout chip with 55micron square elements working in single photon counting mode, IEEE Trans. Nucl. Sci., 49 (2002) 2279-2283.
[25] X.C. Llopart, M First test measurements of a 64k pixel readout chip working in single photon counting mode, Nucl. Instrum. Meth. A, 509 (2003) 157-163.
[26] X. Llopart, R. Ballabriga, M. Campbell, L. Tlustos, W. Wong, Timepix, a 65k programmable pixel readout chip for arrival time, energy and/or photon counting measurements, Nuclear Instruments and Methods in Physics Research Section A: Accelerators, Spectrometers, Detectors and Associated Equipment, 581 (2007) 485-494.
[27] J.M. Vallerga, J.; Tremsin, A.; Siegmund, O.; Mikulec, B.; Clark, A. , Optically sensitive Medipix2 detector for adaptive optics wavefront sensing, Nuclear Instruments and Methods in Physics Research Section A: Accelerators, Spectrometers, Detectors and Associated Equipment, 546 (2005) 263-269.
[28] T.J. Holy, J.; Pospisil, S.; Uher, J.; Vavrik, D.; Vykydal, Z. , Data acquisition and processing software package for Medipix2, Nucl. Instrum. Meth. A., 1 (2006).
[29] D. Turecek, T. Holy, J. Jakubek, S. Pospisil, Z. Vykydal, Pixelman: a multi-platform data acquisition and processing software package for Medipix2, Timepix and Medipix3 detectors, J. Instrum., 6 (2011).
[30] M. Campbell, 10 years of the Medipix2 Collaboration, Nuclear Instruments and Methods in Physics Research Section A: Accelerators, Spectrometers, Detectors and Associated Equipment, In Press, Corrected Proof.
[31] B.W. Schueler, Microscope imaging by time-of-flight secondary ion mass spectrometry, Microsc. Microanal. M., 3 (1992) 119-139.
[32] Z.V. Vykydal, J.; Sabuncuoglu Tezcan, D.; De Munck, K.; Borgers, T.; Ruythooren, W.; De Moor, P. , The RELAXd project: Development of four-side tilable photon-counting imagers, Nucl. Instrum. Meth. A, 591 (2008) 241-244.
[33] J. Visser, B. van der Heijden, S.J.A. Weijers, R. de Vries, J.L. Visschers, A Gigabit per second read-out system for Medipix Quads, Nuclear Instruments and Methods in Physics Research Section A: Accelerators, Spectrometers, Detectors and Associated Equipment, In Press, Corrected Proof.
[34] D.I. Fries, S.; Broadbent, H.; Willoughby, R.; Sheehan, E.; , Micro Ion-Optical Systems Technology [MIST] for Mass Spectrometry Using PCBMEMS, IEEE International Symposium on Industrial Electronics, 2007. ISIE 2007., (2007) 3278 - 3281.
[35] T. Holy, J. Jakubek, S. Pospisil, J. Uher, D. Vavrik, Z. Vykydal, Data acquisition and processing software package for Medipix2, Nuclear Instruments and Methods in Physics Research Section A: Accelerators, Spectrometers, Detectors and Associated Equipment, 563 (2006) 254-258.

Tables

Table 1: Protein Calibration Standard I and II (Bruker Daltonik GmbH, Bremen, Germany).

Protein	Average m/z	Calibration Standard
Insulin $[M+H]^+$	5,734.51	I
Ubiquitin I $[M+H]^+$	8,565.76	I
Cytochrome C $[M+H]^+$	12,360.97	I
Myoglobin $[M+H]^+$	16,952.30	I
Cytochrome C $[M+H]^{2+}$	6,180.99	I
Myoglobin $[M+H]^{2+}$	8,476.65	I
Typsinogen $[M+H]^+$	23,982	II
Protein A $[M+H]^+$	44,613	II
Albumin-Bovine (BSA) $[M+H]^+$	~66,500	II
Protein A $[M+H]^{2+}$	22,307	II
Albumin-Bovine (BSA) $[M+H]^{2+}$	~33,300	II

Figures

Fig. 1: Schematic representation of the ion microscope mass spectrometer and potential diagram for the operation of the floating Timepix detector assembly in positive and negative ion mode.

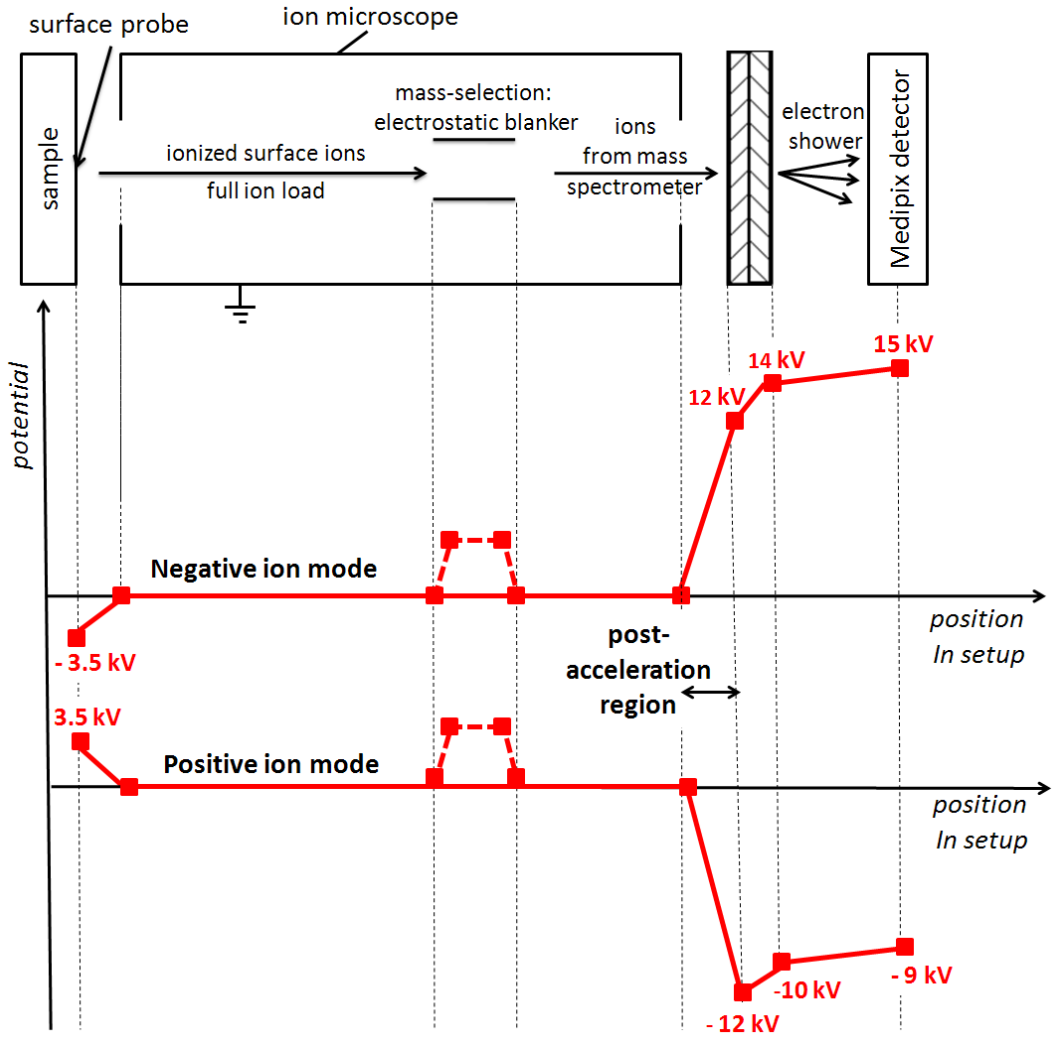

Fig. 2: Schematic representation of the high-vacuum compatible chip carrier. The chip carrier consists of a standard, multilayer FR-4 PCB to which a layer of liquid crystalline polymer (LCP) is applied on both sides. The edge of the board is sealed with a layer of copper and indium to prevent outgassing and to provide a metal surface for the vacuum seal between the carrier and the vacuum chamber of the mass spectrometer.

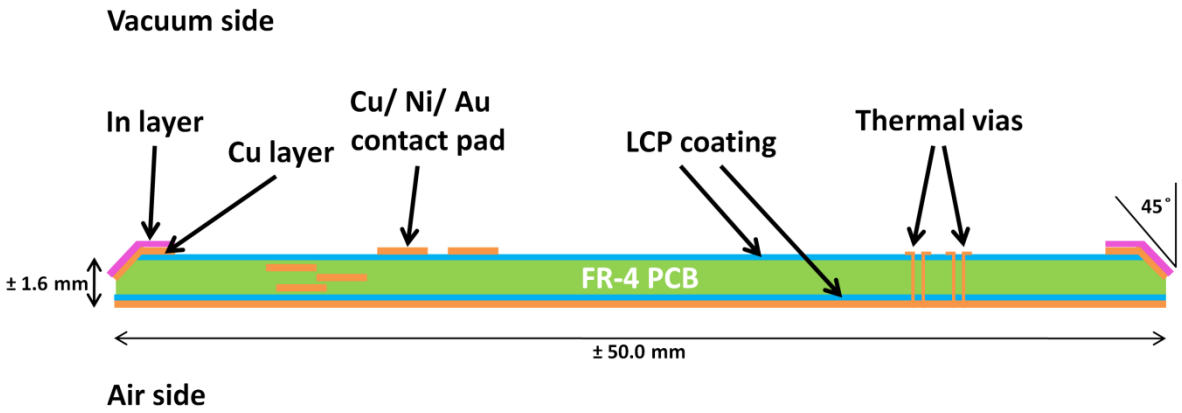

Fig. 3: Photos of the high-vacuum compatible chip carrier glued into the stainless steel support. (a) In-vacuum (front) side of the carrier. The four drilled and threaded holes mark the positions on which the MCP support will be attached. (b) In-air (back) side of the chip carrier. The copper block provides mechanical support and functions as a heat sink. The readout interface board can be clicked into the connector located in the center of the chip carrier. (c) Zoom on the bonding pads and wire-bonded chips on the in-vacuum side.

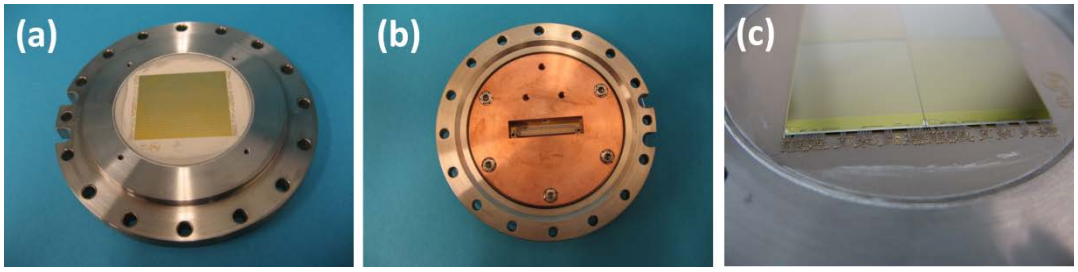

Fig. 4: (a) Mass spectra of the protein calibration standard in the mass range from 0-15 kDa acquired in negative ion mode at an ion post-acceleration voltage of 4 keV (blue), 7 keV (green), 10 keV (red) and 13 keV (black). (b) Mass spectra of the protein calibration standard in the mass range from 0-15 kDa acquired in negative ion mode at an ion post-acceleration voltage of 7 keV (green), 10 keV (red) and 13 keV (black). (c) Mass spectra of the protein calibration standard in the mass range from 0-14.5 kDa acquired in positive ion mode at an ion post-acceleration voltage of 5.5 keV (blue), 8 keV (green), 10.5 keV (red), 13 keV (black). (d) Time-of-flight spectrum of the protein calibration standard in the mass range of about 10-18 kDa acquired in positive ion mode at an ion post-acceleration voltage of 5.5 keV (blue), 8 keV (green), 10.5 keV (red) and 13 keV (black).

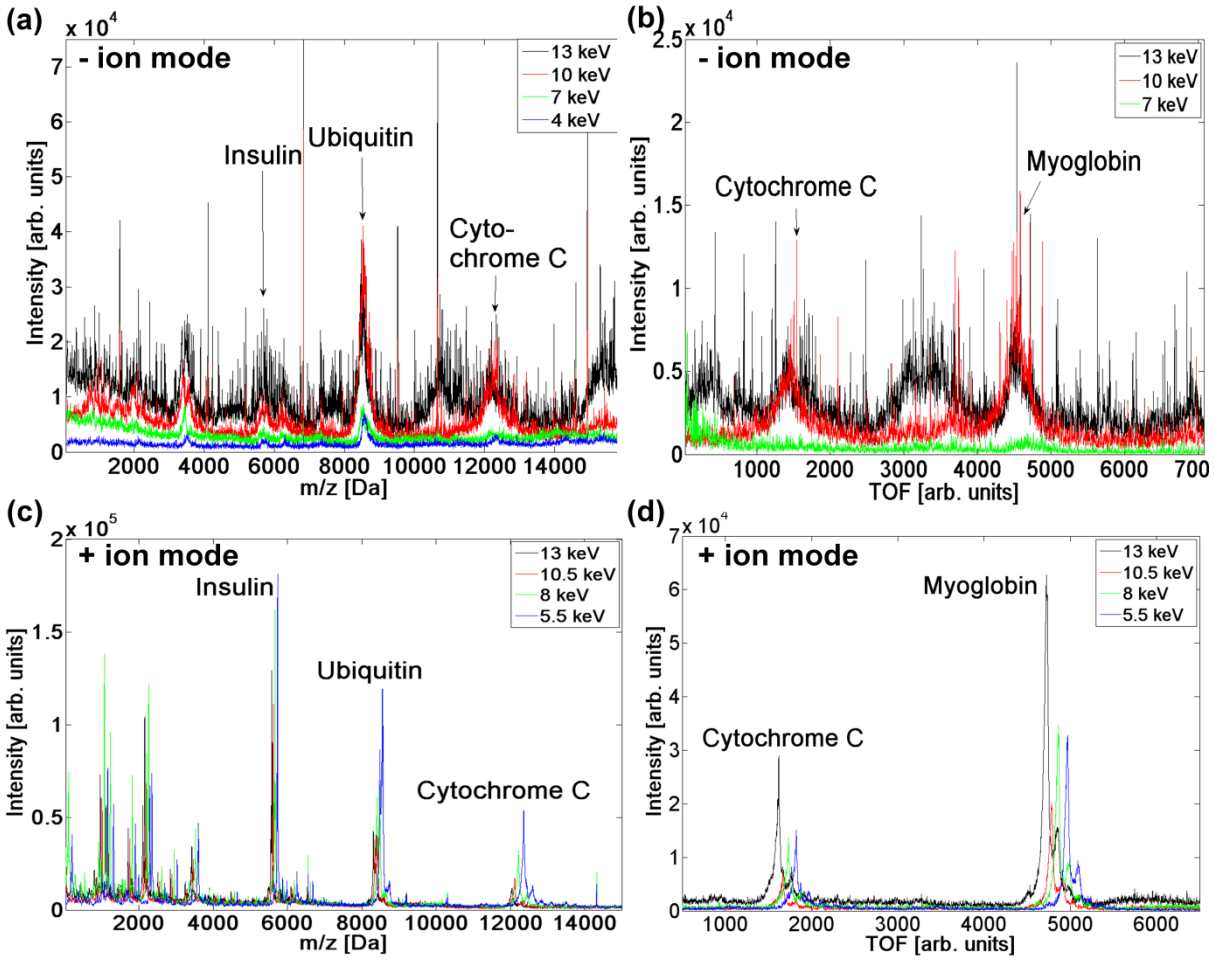

Fig. 5: Spectra of the protein calibration standard in the mass range up to 70 kDa. The spectra are acquired with the Timepix detection system on the TRIFT ion microscope at ion acceleration energies of 5.5 keV (black) and 10.5 keV (red). The green arrows indicate where consecutive Timepix-generated spectra were stitched together. The inset shows a zoom on the mass range from 30 to 65 kDa.

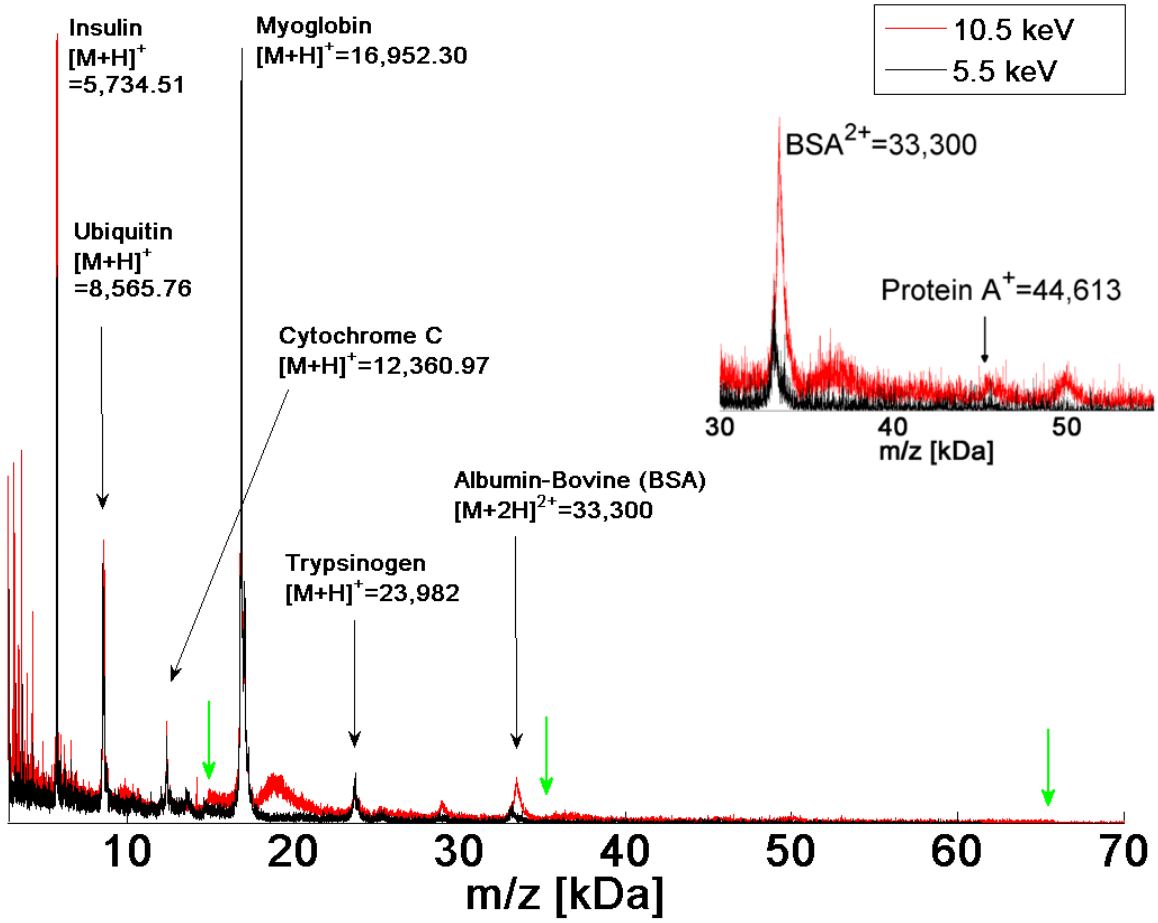

Fig. 6: Spectra of the protein ubiquitin in the mass range up to 100 kDa. The spectra are acquired with the Timepix detection system on the TRIFT ion microscope at ion acceleration energies of 5.5 keV (black) and 10.5 keV (red). The green arrows indicate where consecutive Timepix-generated spectra were stitched together. The inset displays a zoom on the mass range from 55 to 100 kDa.

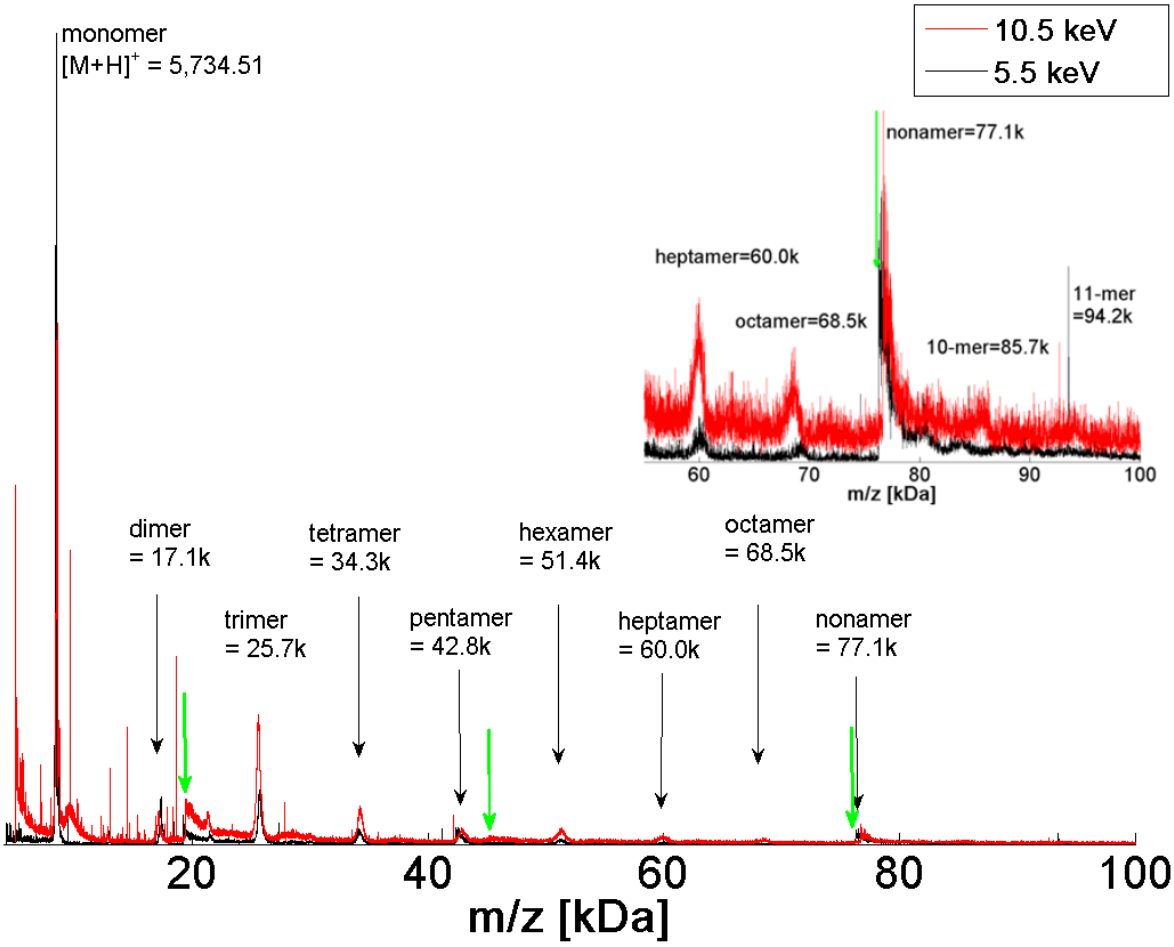

Appendices

Appendix A

Fig. A.1: Representation of the mechanical design of the HV setup. The inner shell contains the detection system, readout board, temperature control system and signal-converter at high voltage. The outer shell functions as a protective housing. The most crucial elements of the setup are annotated.

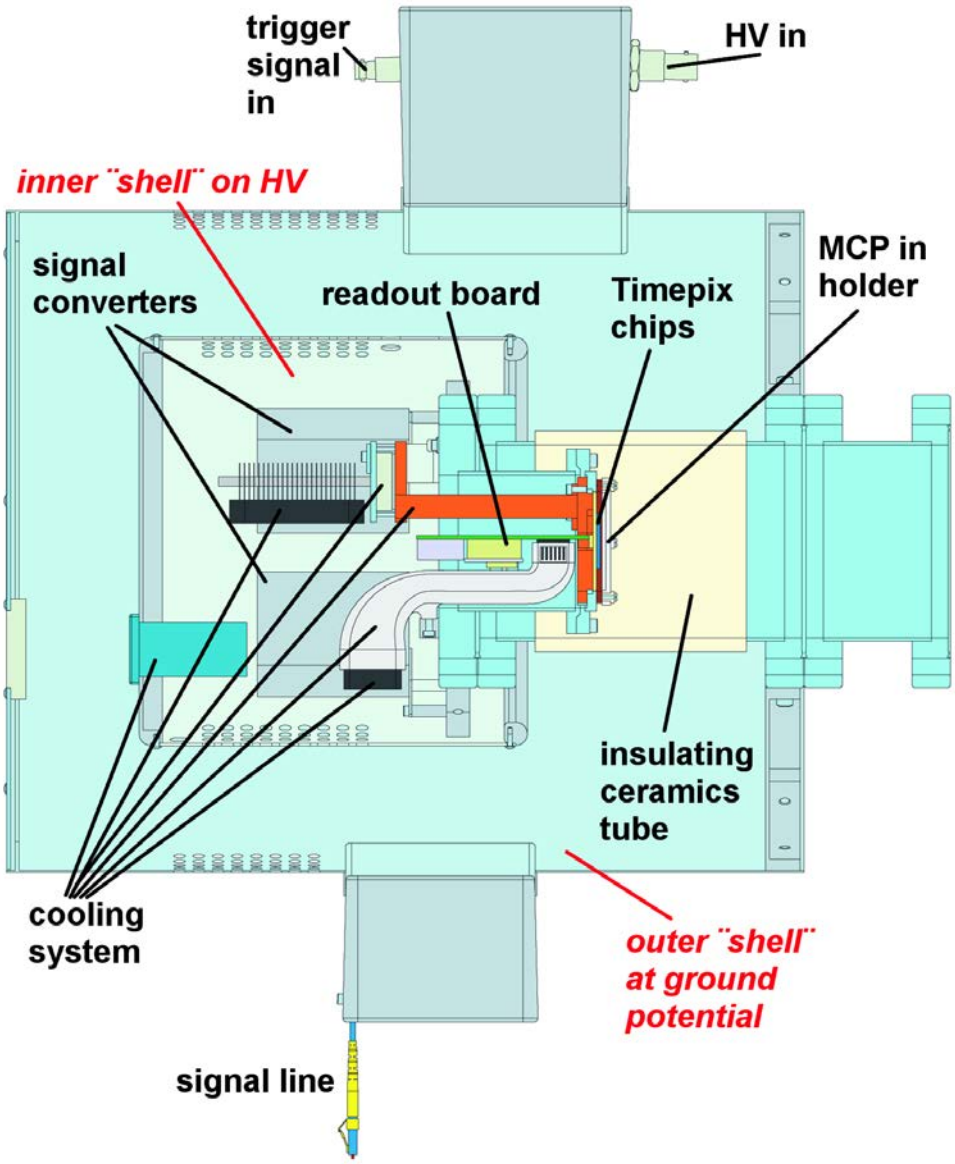

Fig. A.2: Schematic representation of the electrical design of the high voltage setup. The electronics inside the shaded box is floating on HV and is physically contained within the inner shell of the mechanical design (Fig. 7.2). The electronics outside the shaded box are at ground potential and are located outside the outer protection shell of the setup.

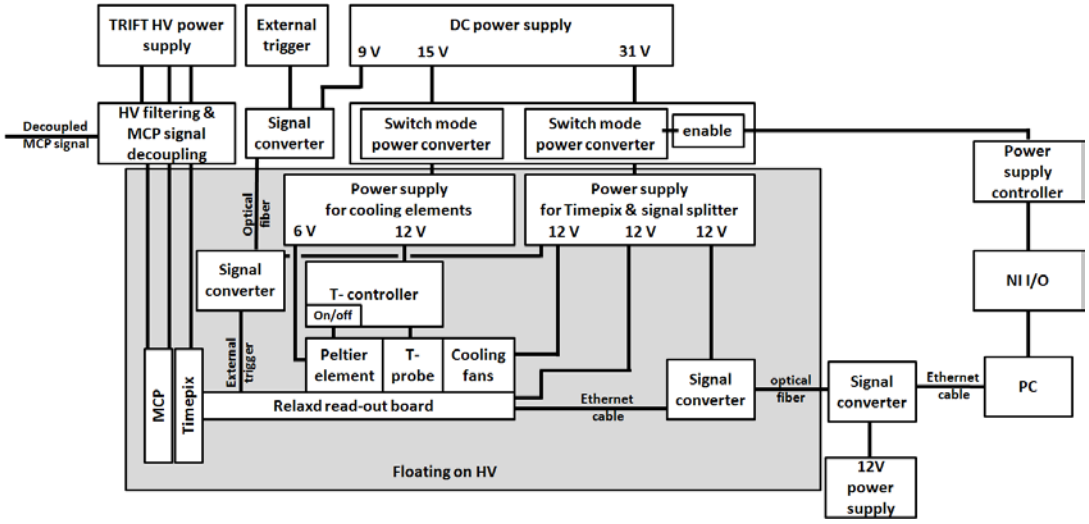

Appendix B

Active Peltier Cooling System. The four Timepix chips dissipate approximately 4 W in total. Therefore, the in-vacuum mounting of the Timepix chips requires active cooling to prevent overheating. In the presented setup, the chips are cooled actively with two Peltier elements. The Peltier elements and the chips are connected by a series of copper parts. The assembled chip carrier is glued to the copper support/heat sink with thermally conducting glue. The copper heat sink is connected to a copper heat conductor that terminates in a platform on which the two Peltier elements are installed (PE-127-10-13-S, sealed, 37.2 W cooling power at T=0 and maximum current=3.9 A, maximum T=70 ^{o}C at maximum current=3.9 A and power=0; Global Component Sourcing, Hong Kong). The Peltier elements are cooled with a heat sink and a fan. The cooling temperature is probed with a PT-100 temperature probe, which is attached to the copper platform next to the Peltier elements. The cooling platform temperature is controlled and held at a given set point, typically 8 ^{o}C, with a temperature controller (eTRON M electronic microstat, JUMO GmbH & Co. KG, Fulda, Germany). The temperature of the chips is monitored via the Max6642 temperature sensor, which is located in the chip carrier PCB below the four chips. The field-programmable gate array (FPGA) on the readout board is cooled with a fan (via a cooling tube). The FPGA temperature is also given by the Max6642 which reads a FPGA-internal sensor diode. The chip and the FPGA temperature readings are transferred to the measurement personal computer (PC) via the Ethernet readout connection. A dedicated temperature monitoring and control software was developed. This software package was incorporated into the Medipix/Timepix readout software Pixelman (Pixelman software, version 2010/03/29, [29, 35]) as a “plug-in". The temperature monitoring and control software (system overview in Fig. 6) grabs the chip and FPGA temperature readings from the Ethernet data stream and displays the temperature readings in a graphical user interface (GUI) window. In the GUI, the user can specify an “alarm" and a “switch-off" temperature (0<alarm/switch-off temperature<100 ^{o}C) for the chips. If the chip temperature reading is higher than the user-specified alarm temperature for a user-set amount of time (0<alarm time-out<100 s), the GUI goes into alarm status (turns red) and an acoustic alarm sets in. Once the chip temperature exceeds this switch off temperature for a user-set period of time (0<alarm timeout <100 s), the software is capable of shutting down the chips' and readout board's power supplies to prevent overheating. The switch-off procedure is enabled via a multifunction DAQ unit (NI USB-6008, 12-Bit, 10 kS/s Low-Cost Multifunction DAQ, National Instruments, Austin, USA) and a home-made power supply controller, which converts the TTL signal from the NI I/O into a “disable" signal for the Timepix and ReLAXD board power supplies. Typically, the system is operated at an “alarm" temperature of 35 ^{o}C and a “switch off" temperature of 45 ^{o}C. The software writes the chip and FPGA temperatures as well as the user-set “alarm" and “switch off” temperatures to a log file. This temperature control program enables unattended measurements, which is convenient for long and/or over-night experiments.

Fig. B.1: Schematic representation of the hardware components and software working mechanism of the temperature monitoring and control implemented for this setup.

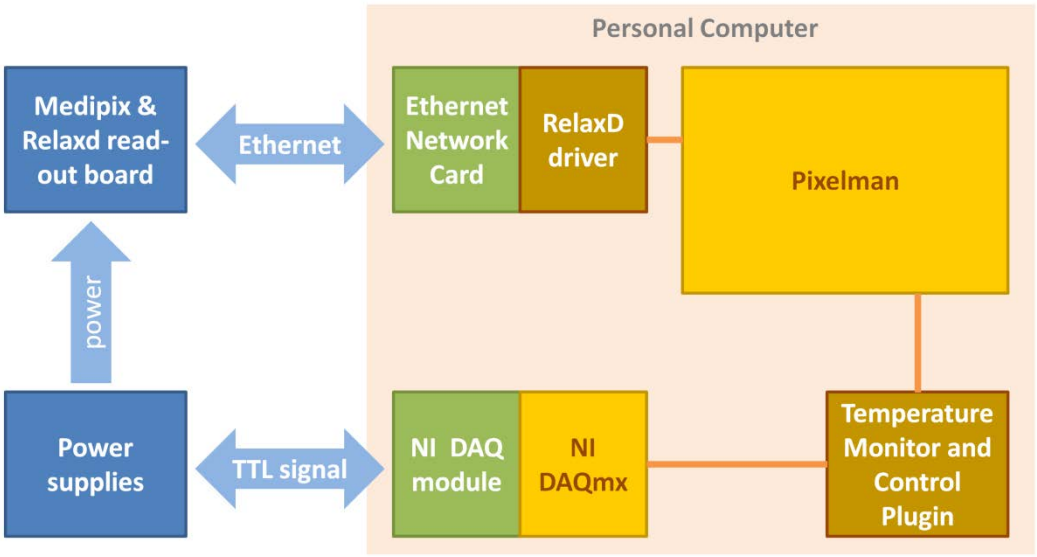

Appendix C

Fig. C.1: Protein calibration standard spectra acquired with a TDC on the TRIFT ion microscope. The spectra are acquired at ion acceleration energies of 5.5 keV (green), 8 keV (red) and 10.5 keV (blue).

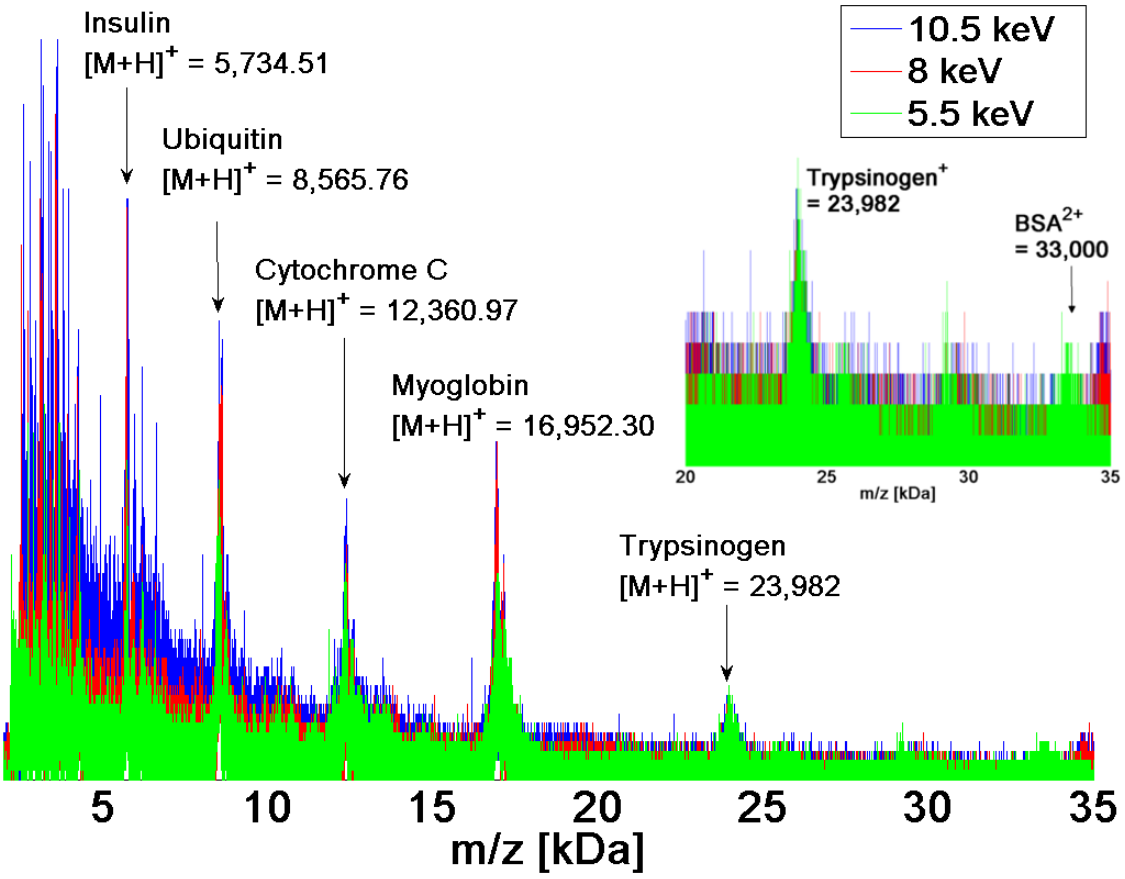

Fig. C.2: Spectra of the protein calibration standard in the mass range up to 70 kDa. The spectrum is acquired with a Ultraflex III spectrometer.